



Splitting capacity of *Eucalyptus globulus* beams loaded perpendicular to the grain by connections

Almudena Majano-Majano · Antonio José Lara-Bocanegra · José Xavier · Manuel Guaita

Received: 18 December 2021 / Accepted: 11 May 2022 / Published online: 5 June 2022
© The Author(s) 2022

Abstract In timber structures, knowledge of the splitting capacity of beams loaded perpendicular to the grain by dowel-type connections is of primordial importance since brittle failure can occur. In the present work, single- and double-dowel-type connections following different loaded edged distance arrangements are experimentally investigated to derive the splitting behaviour of *Eucalyptus globulus* L., which is a hardwood species of increasing interest for structural use due to its high mechanical performance, fast growth, and good natural durability. The correlation of experimental failure loads with those theoretically predicted by the expression included in

Eurocode 5 and by eight analytical models based on an energetic approach is discussed. Most of the analytical models studied overpredict the splitting capacity. However, the code splitting expression, derived from softwoods, proves to be very conservative in predicting the eucalyptus splitting failure load.

Keywords Dowel joint · Hardwood · Blue gum · Fracture energy · Analytical model

1 Introduction

Nowadays, there is growing environmental awareness and increasing demands for sustainability, in response to which wood is established as one of the most suitable materials for building as a natural and renewable resource.

Although the vast majority of products used in timber engineering are made of softwoods, hardwood species are gaining increasing attention for structural applications in the European market. This is mainly due to the large stocks of structurally unused hardwood resources in Central and Southern Europe, to the shortage of softwoods and consequent higher costs, and to continuous changes in reforestation policies toward hardwoods due to the greater suitability of several broadleaf species for soil and climate conditions [1]. This interest is demonstrated by emerging

A. Majano-Majano (✉) · A. J. Lara-Bocanegra
Department of Building Structures and Physics, School of Architecture, Universidad Politécnica de Madrid, Avda. Juan de Herrera, 4, 28040 Madrid, Spain
e-mail: almudena.majano@upm.es

A. J. Lara-Bocanegra
e-mail: antoniojose.lara@upm.es

J. Xavier
UNIDEMI, Department of Mechanical and Industrial Engineering, Faculty of Sciences and Technology, NOVA University of Lisbon, 2928-516 Caparica, Portugal
e-mail: jmc.xavier@fct.unl.pt

M. Guaita
Department of Agroforestry Engineering, University of Santiago de Compostela, Calle Benigno Ledo, 27002 Lugo, Spain
e-mail: m.guaita@usc.es



hardwood products, mainly glued laminated products [e.g., 2–4].

In this regard, *Eucalyptus globulus* Labill (also known as southern blue gum) stands out as a high-performance hardwood of significant interest, due to its fast growth, high mechanical properties, and good natural durability. Recently, there has been increasing industrial and institutional interest driving scientific research on *E. globulus* in different fields, such as silviculture [5–8], mechanical characterisation of the material with small clear specimens [9, 10] and structural size [11, 12], performance of bonded joints for laminated products [13, 14], as well as research related to the development of higher added value building and engineering wood products using this species, such as finger-jointed solid timber [11], glued laminated timber [15], cross-laminated timber (CLT) [16, 17], laminated veneer lumber (LVL) and plywood [18–20] or nail-laminated timber (NLT) and NLT-concrete composite floor panels [21].

In the last century, eucalyptus has become one of the most widely cultivated fast-growing species worldwide in forestry exploitations for production purposes, mainly focused on pulp and paper industries. The *Eucalyptus globulus* species is the most dominant hardwood plantation in Australia together with *Eucalyptus nitens* [22]. It is also one of the main hardwood species in South America. The Iberian Peninsula (Europe) hosts the most extensive *E. globulus* plantations, distributed primarily along the western and northern coasts, comprising Portugal and northern Spain [23].

In Europe, *Eucalyptus globulus* is assigned to the D40 strength class for structural use according to the European standard EN 1912:2012 [24]. The Spanish visual grading standard UNE 56546:2013 [25] only applies to *E. globulus* solid wood with maximum cross-sections of $60 \times 200 \text{ mm}^2$ because, in practice, larger cross-sections are difficult to obtain due to drying problems. For such larger cross-sections, glued laminated products would be a choice.

Thanks to the high performance of this species, eucalyptus solid timber or finger jointed solid timber with small cross-sections could be used in efficient structures, such as trusses, lattice structures, or gridshells [11, 26]. The timber elements that form these structures are often joined by dowel-type connections, which, if loaded perpendicular to the grain, may lead to brittle splitting failure of the timber member at load

levels below the bearing capacity required for desirable ductile behaviour [27] (as is well known, the strength and stiffness perpendicular to the grain are particularly low in wood). Therefore, this brittle failure is one of the most critical in timber structures and deserves special attention in design to achieve adequate reliability.

Most design codes for timber structures currently include explicit expressions to quantify the splitting capacity of connections. These approaches are mainly based on a strength criterion (the former German DIN 1052:2008 [28] based on Ehlbeck et al. [29]) or on an energetic approach within the framework of fracture mechanics (Eurocode 5 [30], Canadian OS86:19 [31]).

In particular, the expression adopted in Eurocode 5 describing the splitting capacity of a connection loaded perpendicular to grain by means of fasteners other than punched metal plates is a quite simple formula applicable only to softwoods, which considers only geometrical parameters (the dimension of the beam cross-section and the distance from the fastener to the loaded edge of the beam). The expression is based on the analytical model originally formulated by Van der Put [32] in the framework of linear elastic fracture mechanics (with a further publication by Van der Put and Leijten [33] in an effort to make the theory more transparent).

As a drawback to its simplicity, the Eurocode 5 splitting capacity expression does not consider the influence of important parameters such as connection layout, type and number of fasteners, different loading cases, etc. Ongoing research has been addressed to propose alternative analytical expressions in order to extend or adapt the original expression, considering to a greater or lesser extent the effect of different geometrical and material parameters based on experimental tests or numerical analysis [34–40]. However, there is no general agreement between the results and the expression derived by Van der Put and Leijten still remains in the code. A comprehensive review of existing approaches can be found in Schoenmakers [41] and Jockwer and Dietsch [42].

Both the original van der Put and Leijten equation and the analytical variants based on fracture mechanics proposed in the literature consider the material fracture energy in their formulations, whereas the strength approaches are based on tensile strength perpendicular to the grain as a material property. There is no compilation of fracture energies for the



different species in the standards, but this property must be obtained experimentally. The fracture energies in Modes I and II loading of *E. globulus* have been achieved in previous work by the authors [43–45]. However, there are no studies on the splitting capacity in eucalyptus.

Furthermore, as mentioned above, the Eurocode 5 expression is only applicable to softwoods. Most subsequent research has also focused mainly on solid wood or timber products with softwoods. Therefore, the suitability to hardwood species of this or other analytical proposals in the literature requires particular research, considering that hardwoods show greater mechanical properties than softwoods, including higher fracture energy and higher tensile strength perpendicular to the grain. Therefore, the use of expressions calibrated for softwoods might be too conservative for hardwoods.

The aim of the present work was to study, for the first time to the best of the authors' knowledge, the splitting capacity of *Eucalyptus globulus* L. solid wood loaded perpendicular to the grain by steel dowel-type connections. Experimental tests were carried out on beams with single and double dowel connections placed at different loaded edge distances to derive the splitting capacity of this species. The adequacy to eucalyptus hardwood of the expression included in Eurocode 5 for softwoods was discussed. The correlation between experimental splitting failure loads and those predicted theoretically by different analytical models from the literature based on the experimentally determined fracture energy of the material was also addressed.

2 Materials and methods

2.1 Material properties

7 boards of *Eucalyptus globulus* Labill. from the Galicia region of northern Spain were used to prepare the 32 specimens used in the splitting tests (Sect. 2.2). All boards met the visual classification criteria of the Spanish standard UNE 56546:2013 [25]. It should be noted that the boards were approximately free of knots. This is usually the case in *E. globulus* because it develops a natural pruning, so from the starting point the knots are few and very small. The boards were conditioned at 20 °C and 65% relative humidity prior

to specimen preparation, reaching an equilibrium moisture content of 12.8%.

The 7 boards were subjected to edgewise bending tests under four-point loading according to EN 408:2011 [46] to obtain their static longitudinal modulus of elasticity (E_L). The boards were planed before testing to a final dimension of $29 \times 116 \times 3042 \text{ mm}^3$. The test span was set at 18 times the depth (width of cross-section). Table 1 shows the result obtained for each board (identified with a reference number that will also identify the splitting specimens to be extracted from each of them). Table 1 also includes the densities (ρ) determined from its dimensions and total weight for a reference moisture content of 12%.

The mechanical properties of the material required in the different analytical models for the splitting analysis carried out in the present work (see Sect. 3) are the longitudinal modulus of elasticity (E_L), the shear modulus of elasticity in the LR plane (G_{LR}), the tensile strength perpendicular to the grain ($f_{t,90}$), and the fracture energy in Mode I loading in most of the models (G_{Ic}) and in Mode II (G_{IIc}).

The E_L value of each splitting specimen was taken from the board from which it was extracted. The rest of the material properties (G_{LR} , $f_{t,90}$, G_{Ic} and G_{IIc}) were taken from previous experimental work by the authors.

Specifically, for the determination of G_{LR} and $f_{t,90}$, eucalyptus boards with similar E_L and ρ to those referred to above were used. A mean value of $G_{LR} = 1926 \text{ MPa}$ was obtained from compression tests on ten small clear specimens [9] and a mean value of $f_{t,90} = 7.5 \text{ MPa}$ from perpendicular-to-grain tensile tests on thirty-six specimens [10].

Table 1 Density and longitudinal modulus of elasticity of *E. globulus* boards

| Board reference | ρ (kg/m ³) | E_L (MPa) |
|-----------------|-----------------------------|-------------|
| 143 | 787 | 20777 |
| 154 | 840 | 18592 |
| 168 | 754 | 19967 |
| 183 | 777 | 18277 |
| 184 | 829 | 18502 |
| 187 | 788 | 19028 |
| 188 | 848 | 20169 |

Regarding the fracture properties of *E. globulus*, the evaluation of Mode I fracture energy is detailed in [43] and [44] using Double Cantilever Beam (DCB) specimens (Fig. 1a). A mean value of the critical strain energy release rate $G_{Ic} = 0.77$ N/mm was derived from the resistance curves (*R*-curves) following the compliance-based beam method (CBBM) as a data reduction scheme. This method was also applied to determine the critical strain energy release rate in Mode II loading from end-notched flexure (ENF) tests (Fig. 1b), resulting in a mean value of $G_{IIc} = 1.54$ N/mm [45].

Table 2 summarises the mean values of these properties that will be considered in the different analytical models to study the splitting behaviour of *E. globulus*.

2.2 Splitting tests

32 splitting tests were conducted on planed *E. globulus* specimens of 29×116 mm² cross-section, 580 mm length and 500 mm span. This and similar cross-sections are readily available in this species.

Two series of three-point bending tests were carried out on single and double dowel connections with different arrangements of loaded edge distances (h_e):

- (a) A single steel dowel of $d = 16$ mm diameter and of S355 quality placed in the middle of the beam. Three h_e were evaluated: $2d$, $3d$ and $4d$ (32 mm, 48 mm, and 64 mm) (Fig. 2a). The relative height of the connection is sometimes simplified by the parameter α ($= h_e/h$). The configurations mentioned correspond to α values of 0.27, 0.41 and 0.55, respectively (test data reported in the literature have shown that α values up to 0.7 may fail by

splitting [37], with the splitting check restricted to $\alpha \leq 0.7$ in the former German standard [28]). It should be noted that $h_e = 4d$ corresponds to the minimum loaded edge distance set out in Eurocode 5 [30], but there is always the possibility of execution errors when drilling holes on site, which are particularly relevant in structures with small depth elements, such as the ones studied here. Between seven and nine beams were tested for each configuration.

- (b) Two steel dowels in a row of $d = 16$ mm in diameter and quality S355, spaced $3d$ (48 mm) apart between their centres and placed at $h_e = 4d$ (64 mm) as shown schematically in Fig. 2b. Eight beams were tested with this layout.

The diameter of the steel dowels was chosen to be sufficiently thick to prevent yielding. These were loaded by two outer plates made of *Eucalyptus globulus* with characteristics similar to those of the beams (note that no embedment damage occurred in the plates). A load cell of 50 kN maximum capacity was used. The tests were carried out at a constant cross-head displacement rate of the test device, adjusted to reach failure in approximately 5 min (2 mm/min, 1 mm/min and 0.5 mm/min for $h_e = 4d$, $h_e = 3d$ and $h_e = 2d$ layouts, respectively, in the single-dowel tests; 0.7 mm/min velocity in the double-dowel tests). During the loading process, the applied load (P) and the displacement (δ) were recorded. For the latter, two Linear Variable Differential Transformer (LVDT) displacement sensors, Solartron AX/10/S, with ± 10 mm measurement range and 20 mV/V/mm sensitivity, were used: one was located on the middle bottom side of the specimen and the other at the top of the steel dowel.

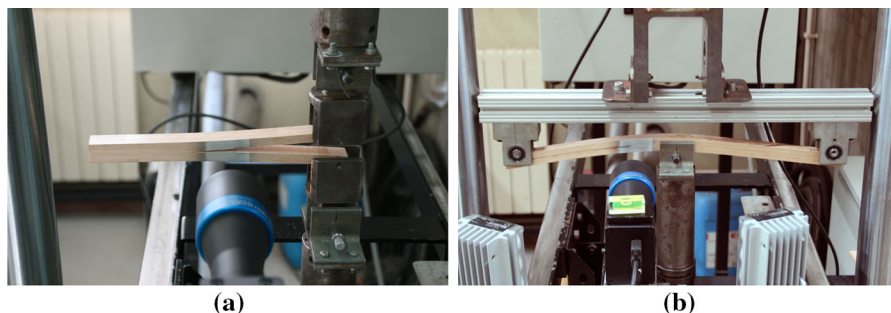
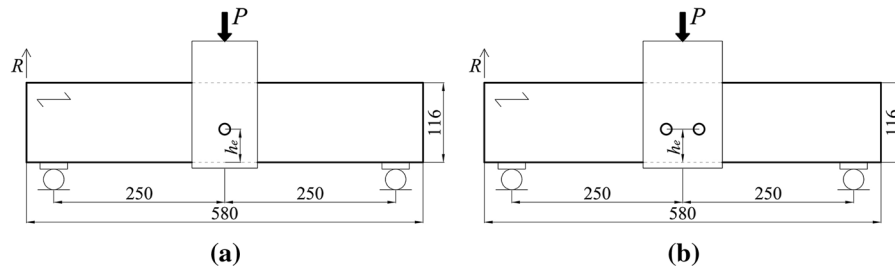


Fig. 1 **a** Double cantilever beam test; **b** end-notched flexure test

Table 2 Number of specimens (n), mean value, and coefficient of variation (CoV) of the different properties of *E. globulus*

| | G_{LR} (N/mm ²) | $f_{t,90}$ (N/mm ²) | G_{Ic} (N/mm) | G_{IIc} (N/mm) |
|---------|-------------------------------|---------------------------------|-----------------|------------------|
| n | 10 | 36 | 13 | 10 |
| Mean | 1926 | 7.5 | 0.77 | 1.54 |
| CoV (%) | 24 | 16 | 23 | 28 |

**Fig. 2** Connection geometries: **a** Single-dowel; **b** double-dowel

3 Analytical models studied

The considered analytical fracture mechanics models for the analysis of the splitting capacity of beams loaded perpendicular to grain by connections are shown in Table 3. A comprehensive review of most of these approaches can be found in [35, 41]. Therefore, in this work, only a summary of these models will be presented. Most of the models are related and appear as special cases of a general one, where the failure load is determined for a linear elastic body loaded with a single force, based on the energy balance approach [47] and the fracture mechanics compliance method according to Eq. (1):

$$P_u = \sqrt{\frac{2G_f}{\frac{dC(A)}{dA}}} \quad (1)$$

being A and C the crack area and the model compliance, respectively.

The different analytical models in Table 3 are derived using Eq. (1) making certain assumptions on how to calculate the compliance $C(A)$, which leads to a good agreement with the experimental data. The external load is assumed to act at a single point in the middle of the beam. The parameters considered by the models are both material and geometrical. The material properties are the fracture energy, G_f (G_{Ic} of the Mode I loading in most models); the shear modulus of elasticity, G ; the longitudinal modulus of elasticity, E ;

and the tensile strength perpendicular to the grain, f_t . The main geometric parameters are the width of the beam, b ; the height of the beam, h ; the distance from the connector to the loaded edge of the beam, h_c ; the relative height of the connection, $\alpha (= h_c/h)$; the shear correction factor, β_s , which takes the value of 6/5 for a rectangular cross-section according to ordinary beam theory; the number of rows of dowels parallel to grain, n ; and the connection width, a_r .

Jensen [34] formulated one of the most general models as an extended version of the original Van der Put and Leijten model [33], which will be discussed below, but without any simplifying assumptions, such as neglecting the normal forces in the cracked parts of the beam. The model was derived considering a cracked beam structure modelled by beam elements, all rigidly connected. The failure load is given by Eq. (2).

Another model which appears as a special case of the model expressed by Eq. (2) was later proposed by Jensen et al. [35], derived this time from considering that the part of the beam below the crack behaves like a beam with fixed ends, of length the crack and depth h_e . The expression is shown in Eq. (3), which would also be arrived at by assuming $h \rightarrow \infty$ for a finite value of h_e (i.e. $\alpha \rightarrow 0$) in Eq. (2), that is, all beams except the beam with depth h_e are assumed to be infinitely stiff.

When only shear deformations are considered and thus bending deformations are neglected (i.e., finite G ,

Table 3 Analytical models for the analysis of the splitting capacity of beams loaded perpendicular to grain by connections

| Reference | Analytical Model | Equation |
|-------------------------------------|---|--------------|
| Jensen (2005a) [34] | $P_u = 2b \sqrt{\frac{2GG_f h_e}{3\beta_s \left(\frac{z}{h_e}\right)^2 (1-\alpha^2) + \beta_s (1-\alpha^2)}}$ | Equation (2) |
| Jensen et al. (2015) [35] | $P_u = 2b \sqrt{\frac{2GG_f h_e}{3\beta_s \left(\frac{z}{h_e}\right)^2 + \beta_s}}$ | Equation (3) |
| Larsen and Gustafsson (2001) [36] | $P_u = 2b \sqrt{\frac{2GG_f h_e}{\beta_s}}; \beta_s = 1$ | Equation (4) |
| Van der Put and Leijten (2000) [33] | $P_u = 2bC_1 \sqrt{\frac{h_e}{1-\frac{h_e}{h}}}; C_1 = \sqrt{\frac{5}{3} GG_f}$ | Equation (5) |
| Ballerini (2004) [37] | $P_u = 2bk \sqrt{\frac{h_e}{1-\alpha^2}} \cdot f_w \cdot f_r; k = \sqrt{\frac{5}{3} GG_f}$ | Equation (6) |
| Jensen (2005b) [38] | $P_u = \gamma P_{u,LEFM}$ | Equation (7) |
| | $P_{u,LEFM} = 2bC_1 \sqrt{h_e}; C_1 = \sqrt{\frac{5}{3} GG_f};$ | |
| | $\gamma = \frac{\sqrt{2\zeta+1}}{\zeta+1}; \zeta = \frac{C_1}{f_r} \sqrt{10 \frac{G}{E} \frac{1}{h_e}}$ | |
| Jensen et al. (2015) [35] | $P_u = \gamma P_{u,LEFM}$ | Equation (8) |
| | $P_{u,LEFM} = 2bC_1 \sqrt{\frac{h_e}{1-\frac{h_e}{h}}}; C_1 = \sqrt{\frac{5}{3} GG_f}$ | |
| | $\gamma = \frac{\sqrt{2\zeta+1}}{\zeta+1}; \zeta = \frac{C_1}{f_r} \sqrt{10 \frac{G}{E} \frac{1}{h_e}}$ | |
| Franke and Quenneville (2011) [39] | $P_u = \frac{b \cdot 10^3}{\left(\frac{G_{I, norm}}{G_{Ic}} + \frac{G_{II, norm}}{G_{IIc}}\right)} k_r$ | Equation (9) |
| | $G_{I, norm} = e^{(h^{-1} (200 - 10h_e h^{-0.25} - a_r))}$ | |
| | $G_{II, norm} = 0.05 + 0.12 \frac{h_e}{h} + 1 \cdot 10^{-3} a_r$ | |
| | $k_r = \begin{cases} 1 & \text{for } n = 1 \\ 0.1 + (\arctan(n))^{0.6} & \text{for } n > 1 \end{cases}$ | |

$E \rightarrow \infty$), the ratio $G/E \rightarrow 0$ and Eq. (3) is reduced to the form expressed in Eq. (4). This expression is similar to the solution proposed by Larsen and Gustafsson [36] when $\beta_s = 1$ is assumed.

A renowned simple analytical model that forms the basis for the design in Eurocode 5 [30] is the one proposed by Van der Put and Leijten [33] expressed in Eq. (5). Due to the similarity in behaviour, the same principle was followed as in the mechanical fracture model for the splitting of beams with notches previously derived by Van der Put [32]. The expression is obtained by analysing the cracked state of a beam under an energy balance approach when the joint load is perpendicular to the grain near the loaded edge, using experimental results from the literature as calibration. Although today it is still the model basis of the normative expression, it has been subject to subsequent alterations and adjustments by different researchers. In this sense, the resulting expression could again be seen as a special case of the general

model presented in Eq. (2) neglecting bending deformations and taking into account only shear deformations (that is, $G/E \rightarrow 0$) and $\beta_s = 6/5$ for rectangular cross-section. In the cases where $h_e/h \rightarrow 0$, the van der Put model would lead back to the solution presented in Eq. (4).

Ballerini [37] proposed a semiempirical model given by Eq. (6), in an effort to better fit the experimental data than using the van der Put and Leijten formula for single-dowel connections. The work also provides an approach for multiple-dowel connections and is further elaborated with parametric numerical analysis by Ballerini and Rizzi [48]. It considers the influence of the connection width and depth using correction functions applied to the single-dowel formula. In particular, the correction factor to account for the influence of the width of the connection is $f_w = 1 + 0.75(l_r + l_l/h) \leq 2.2$, where l_r is the spacing between the dowels and l_l is the distance between the dowel clusters (this correction function



will be applied in the case of double dowel connections studied in the present work).

Jensen postulated other analytical models based on the beam-on-elastic foundation (BEF) [38]. In this case, the crack plane is modelled by springs to which the fracture properties are assigned. After cracking, the beam below the fictitious fracture layer is considered as a beam resting on elastic Winkler springs connected to the upper part, which is assumed to be infinitely rigid (foundation). For a single load acting far from the end of the beam and small crack lengths, the failure load is given by Eq. (7), where γ is the effectiveness factor. Unlike the models mentioned above, this expression includes the tensile strength f_t in the parameter ζ , and the splitting failure load is not proportional to the square root of the fracture energy. Therefore, solutions cannot be encompassed within either linear elastic fracture mechanics (LEFM) or nonlinear fracture mechanics (NLEFM). They belong to quasi-nonlinear fracture mechanics, and LEFM solutions are considered special cases.

Assuming $E \rightarrow \infty$ or $f_t \rightarrow \infty$ in the analytical approach of Eq. (7), the solution $P_u = P_{u,LEFM}$ would be obtained. The same solution could also be derived from Eq. (4) for $\beta_s = 6/5$, and from Eq. (5) when $h_e/h \rightarrow 0$. Therefore, it seems feasible to use, as $P_{u,LEFM}$ in Eq. (7) the linear elastic fracture mechanics solution given by Eq. (5). In this way, the analytical model expressed by Eq. (8) is obtained. When $h_e/h \rightarrow 0$, Eq. (8) leads to Eq. (7), and when $E \rightarrow \infty$ or $f_t \rightarrow \infty$ it becomes Eq. (5). Equation (8) is therefore a semi-empirical generalization of Eq. (7) that considers the effect of the total beam height.

Franke and Quenneville [39] presented a complete approach based on a quadratic failure criterion in which fracture modes I and II for tension and shear are considered using the corresponding fracture energies G_I and G_{II} . It should be noted that virtually all fractures are, in fact, mixed-mode fractures, but the mixed-mode ratio is not considered by the aforementioned compliance method. As the G_I of wood is usually much lower than the G_{II} , the G_I is usually considered in most splitting models as a conservative assumption and reasonably accurate approximation, but the mixed-mode fracture energy would represent the most realistic situation. The Franke and Quenneville formula also takes into account the width of the connection and the number of rows of dowels, and they found that the geometry of the connection

influenced the ratio between fracture modes I and II. The design proposal is given by Eq. (9) as a result of an experimental and numerical investigation by finite element analysis of more than 100 different connection arrangements.

All of the above models are similarly acceptable from a modelling perspective. From a practical design point of view, simple and robust models seem to be more attractive.

4 Results and discussion

4.1 Experimental failure loads

The failure behaviour of the series of specimens with one and two dowels in a row and different distances from the loaded edges subjected to splitting tests is herein presented.

In the single-connection tests, a main crack could always be observed growing from both sides of the dowel (Fig. 3a). This crack developed at slightly different positions, starting at the mid-down part of the dowel contact. The smaller the loaded edge distance, the faster the crack developed with respect to the maximum load capacity. In these test groups, the crack never reached the ends of the beam.

Some of the specimens with the largest loaded edge distance ($4d$) showed embedding deformations under the dowels, but no bending of the dowels, as well as some cracks with small lengths beside the dowel (Fig. 3b). The beams with $2d$ and $3d$ loaded edge distances did not exhibit any significant embedment under the dowels. In any case, the brittle failure was always characterised by one main crack.

Regarding the double-dowel tests, a similar crack growth process was observed as for the single-dowel batches in the sense that just one main crack developed on both sides of the beams. However, in all tests, the crack reached the beam ends, producing a complete separation of the specimen into two parts with a very brittle and sudden failure (Fig. 4a).

No embedment deformations were observed under the two dowels (Fig. 4b, unlike in the case of a single dowel for the same loaded edge distance ($4d$), as the bearing area increases with the two closely spaced dowels.

These failure modes are well represented by the corresponding load versus displacement curves

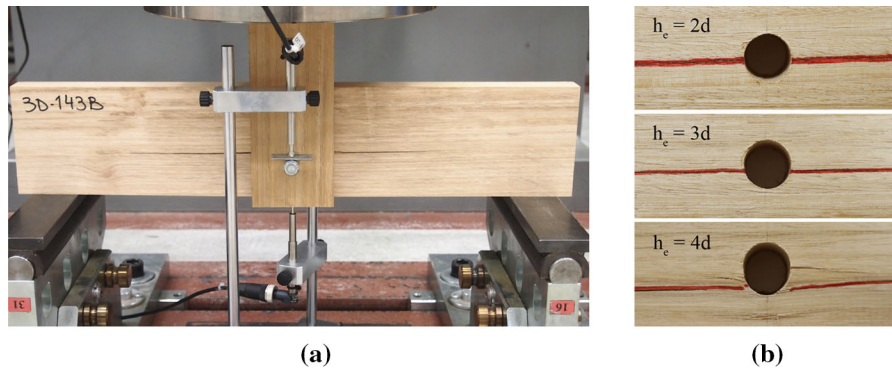


Fig. 3 **a** Representative failure behaviour of single-dowel test series; **b** detail of the local failure around the dowel for the three loaded edge distances



Fig. 4 **a** Representative failure behaviour of the double-dowel test series; **b** detail of local failure around the dowels

measured at the top of the dowels. The results of the single-dowel splitting tests are shown in Fig. 5a, which reveal the different failure behaviour of the investigated connection arrangements.

As can be seen, the load–displacement curves obtained from the beams with the greatest edge

distance ($4d$) show a ductile behaviour characterised by embedment stresses and yielding followed by hardening. The connection is still able to force a splitting failure after considerable slip, although splitting is not the primary failure mode. On the

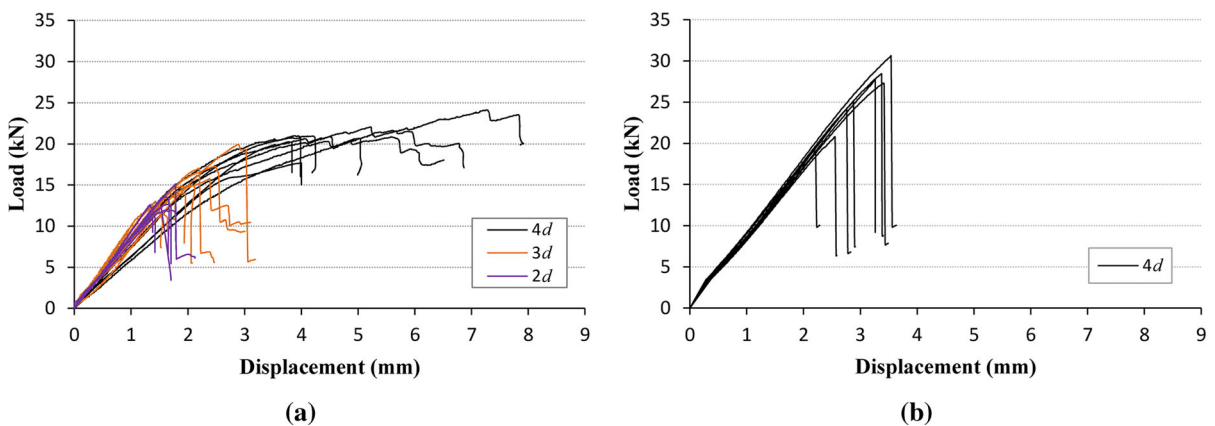


Fig. 5 Load–displacement curves. **a** Single-dowel splitting tests with $2d$, $3d$ and $4d$ loaded edge distances; **b** double-dowel splitting tests with $4d$ loaded edge distance

contrary, a brittle failure response is displayed for lower edge distances ($3d$ and $2d$).

The load–displacement curves of the double-dowel splitting tests with a $4d$ loaded edge distance are shown in Fig. 5b. In this case, a clear brittle behaviour is observed in all specimens for the α -value studied.

Failure loads (P_u) achieved in all splitting tests for the beams with single- and double-dowel arrangements as well as the mean value, the standard deviation (SD) and the coefficient of variation (CoV) are compiled in Table 4.

As can be seen from the results of the single-dowel beams, the load-carrying capacity increases with increasing loaded edge distance.

The failure loads reached by the beams with two dowels are not necessarily twice as high as those achieved by the beams with a single dowel arrangement at the same loaded edge distance $4d$ ($\alpha = 0.55$), but the mean value is only slightly higher (21% higher). These results are in agreement with those obtained by Quenneville and Mohammad [49], who tested different connection arrangements on spruce-pine glulam beams, including series of one and two fasteners spaced horizontally $5d$ apart, with $\alpha = 0.6$. The mean maximum loads in the case of double fasteners were found to be 23% higher compared to the single connection. Previous experimental investigations by Reshke [50] for the same material and joint geometry as specified for [49], also resulted in a small difference of approximately 14% higher failure load

for specimens with two dowels compared to those with one dowel.

The fact that two closely spaced dowels give basically the same splitting failure load as a single dowel was also stated by Kasim and Quenneville [51] using the concept of cluster (group) of fasteners. In their research, the capacity of two rows of bolts separated $4d$ in the direction parallel to the grain turned out to be lower or statistically not different from that of one row of bolts on spruce glulam beams with $\alpha = 0.44$ and $\alpha = 0.70$. As the spacing of the rows increased, so did the splitting capacity of the connection. The two-row joint behaved almost as two separate single rows if the spacing between the rows was $\geq 2h_e$ (75% of twice the capacity of the one-row connection was obtained). The angle of load distribution from a bolt towards the loaded edge was estimated to be 45° . In this regard, the former German code [28] limited to less than $0.5h$ the distance between groups of fasteners in the direction parallel to the grain to be considered as one group. For distances $\geq 2h$ between them, they are treated as separate groups. For distances between $0.5h$ and $2h$, the groups are considered as one group, but a reduction factor is applied. Quenneville and Mohammad [49] stated that a connection can be assumed to be one cluster if the distance parallel to the grain between the rows of bolts does not exceed h_e . The assumed angle of load distribution was 63° in this case.

Table 4 Failure loads from the single- and double-dowel splitting tests

| 1 dowel | | 2 dowels | | | | | |
|--------------------|------------|--------------------|------------|--------------------|------------|--------------------|------------|
| $h_e = 2d = 32$ mm | | $h_e = 3d = 48$ mm | | $h_e = 4d = 64$ mm | | $h_e = 4d = 64$ mm | |
| name | P_u (kN) | name | P_u (kN) | name | P_u (kN) | name | P_u (kN) |
| 168a | 12.30 | 143a | 12.68 | 188a | 22.05 | 183a | 20.80 |
| 168b | 12.57 | 143b | 13.96 | 188b | 20.87 | 183b | 28.42 |
| 168d | 13.46 | 143c | 13.92 | 188c | 24.13 | 183c | 24.18 |
| 168e | 12.67 | 143d | 12.55 | 188d | 21.00 | 183d | 27.25 |
| 184a | 11.21 | 143e | 14.87 | 188e | 20.85 | 183e | 30.61 |
| 184b | 11.88 | 154a | 19.88 | 187a | 20.24 | 184a | 27.65 |
| 184c | 15.09 | 154b | 17.24 | 187b | 17.64 | 187f | 25.12 |
| | | 154c | 16.99 | 187c | 20.74 | 187g | 18.90 |
| | | 154d | 15.74 | | | | |
| Mean | 12.74 | | 15.31 | | 20.94 | | 25.37 |
| SD | 1.25 | | 2.40 | | 1.80 | | 3.96 |
| CoV (%) | 9.8 | | 15.7 | | 8.6 | | 15.6 |



4.2 Comparison of theoretical and experimental failure loads

The adequacy of the different analytical models compiled in Sect. 3 based on fracture mechanics for the prediction of the splitting capacity in timber connections loaded perpendicular to the grain in relation to the experimental data obtained for eucalyptus is discussed here. The material properties E_L , G_{LR} , G_{IC} , G_{IIc} and $f_{t,90}$ experimentally determined for this species (Sect. 2.1) were used as input parameters in the corresponding models.

The ratios of the theoretically predicted failure loads to the experimental values for the single connection arrangement are presented in Table 5. These ratios normalise the strength estimates, allowing for easier comparison. Ratio < 1 represents a conservatively predicted connection strength; ratio ≈ 1 means an accurately predicted connection strength; and ratio > 1 depicts an overpredicted connection strength.

Figure 6 shows graphically these failure load ratios for the single-dowel connection. The results of the $h_e = 2d$ specimens are represented in red, $h_e = 3d$ in blue, and $h_e = 4d$ in green. The results of each analytical model compiled in Table 3 are represented by a different symbol.

As can be observed from Table 5 and Fig. 6, most analytical models overpredict the splitting capacity for single-dowel beams of eucalyptus, which could lead to a dangerous design situation.

The models given by Eqs. (2) and (5) produce the worst predictions in single-dowel specimens (it should be noted that Eq. (5) is the basis for the Eurocode 5 splitting capacity formula). This performance is in line with that obtained by Jensen et al. [35] in research using Radiata pine LVL beams. In such research, Eqs. (2) and (5) did not lead to good agreement with the experimental data if the fracture energy obtained by the single edge notched beam (SENB) fracture tests was used directly. However, the agreement was fair if the fracture energy estimated from plate specimen tests was used instead, as its formulation is closely related to the models given by these two equations. This fact seems to suggest that the linear fracture mechanics model, on which Eqs. (2) and (5) are based on, may have some shortcomings.

The models given by Eqs. (3) and (4) provide better predictions than Eqs. (2) and (5) but still

overestimated. It is worth noting that the former are just special cases of the latter. A similar overestimation is also found by the semiempirical Ballerini model expressed by Eq. (6).

Equation (7) stands out with the best predictions of experimental results in eucalyptus from all models related to the original Van der Put and Leijten equation, where only Mode I is taken into account in terms of fracture energy (Eqs. (2)–(8)). These findings are in line with those of Hindman et al. [52] and Patel and Hindman [53], who concluded that Eq. (7) performed better than Eq. (5) for Southern pine machined stress rated (MSR) lumber, laminated veneer lumber (LVL) composed mostly of southern pine with some eucalyptus, and also for yellow poplar parallel strand lumber (PSL). This can be justified by the fact that in Eq. (7), the tensile strength perpendicular to the grain of the member is added besides the fracture energy. It is worth remembering that Eq. (7) is enclosed within quasi-nonlinear fracture mechanics and the LEFM model described by Eq. (5) could be considered a special case of it.

Equation (8) also includes the tensile strength perpendicular to the grain, and it should be recalled that it was postulated as a semi-empirical modification of Eq. (7) to take into account the total height of the beam. Thus, in the work of the authors who formulated this model [35], Eqs. (7) and (8) gave similar predictions on Radiata pine LVL beams with two dowels aligned along the grain, when the distance to the loaded edge was $4d$ ($\alpha = 0.21$). However, for larger loaded edge distances of $8d$ ($\alpha = 0.43$), predictions from Eq. (8) were clearly better. However, this improvement in results using Eq. (8) instead of (7) is not satisfied in the eucalyptus beams of the present study for any configuration of loaded edge distances in single-dowel joints (nor in beams with two dowels, as will be seen below).

The only model that provides a conservative prediction of splitting failure for most of the eucalyptus specimens tested with a single dowel connection is the one presented by Franke and Quenneville (Eq. (9)) [39], which, unlike the previous ones, also considers the fracture energy in Mode II as a material parameter. In this respect, the authors stated that the fracture values achieved showed that the geometry of the connection, the distance from the loaded edge, and the depth of the beam influence the relationship between fracture Mode I and Mode II.



Table 5 Theoretical vs. experimental failure load ratios of single-dowel connection tests

| h_e (mm) | name | Equation (3) | Equation (4) | Equation (2), Equation (5) | Equation (6) | Equation (7) | Equation (8) | Equation (9) |
|---------------|------------|--------------|--------------|-------------------------------|--------------|--------------|--------------|--------------|
| 2d = 32 | 168a | 1.33 | 1.45 | 1.56 | 1.34 | 1.12 | 1.32 | 0.74 |
| | 168b | 1.30 | 1.42 | 1.52 | 1.31 | 1.10 | 1.29 | 0.72 |
| | 168d | 1.21 | 1.33 | 1.42 | 1.23 | 1.02 | 1.20 | 0.67 |
| | 168e | 1.29 | 1.41 | 1.51 | 1.30 | 1.09 | 1.28 | 0.72 |
| | 184a | 1.46 | 1.59 | 1.71 | 1.47 | 1.22 | 1.43 | 0.81 |
| | 184b | 1.37 | 1.50 | 1.61 | 1.39 | 1.15 | 1.35 | 0.76 |
| | 184c | 1.08 | 1.18 | 1.27 | 1.09 | 0.91 | 1.07 | 0.60 |
| | mean | 1.29 | 1.41 | 1.52 | 1.30 | 1.09 | 1.28 | 0.72 |
| | SD | 0.12 | 0.13 | 0.14 | 0.12 | 0.10 | 0.12 | 0.07 |
| | CoV (%) | 9.3 | 9.3 | 9.3 | 9.3 | 9.2 | 9.2 | 9.3 |
| | 3d = 48 | 143a | 1.58 | 1.73 | 2.06 | 1.63 | 1.38 | 1.81 |
| 143b | | 1.43 | 1.57 | 1.87 | 1.48 | 1.26 | 1.64 | 0.98 |
| 143c | | 1.43 | 1.57 | 1.87 | 1.49 | 1.26 | 1.64 | 0.98 |
| 143d | | 1.59 | 1.74 | 2.08 | 1.65 | 1.40 | 1.82 | 1.09 |
| 143e | | 1.34 | 1.47 | 1.75 | 1.39 | 1.18 | 1.54 | 0.92 |
| 154a | | 1.00 | 1.10 | 1.31 | 1.04 | 0.87 | 1.14 | 0.69 |
| 154b | | 1.16 | 1.27 | 1.51 | 1.20 | 1.01 | 1.32 | 0.79 |
| 154c | | 1.18 | 1.29 | 1.54 | 1.22 | 1.02 | 1.34 | 0.80 |
| 154d | | 1.27 | 1.39 | 1.66 | 1.32 | 1.10 | 1.44 | 0.87 |
| mean | | 1.33 | 1.46 | 1.74 | 1.38 | 1.16 | 1.52 | 0.91 |
| SD | | 0.20 | 0.22 | 0.26 | 0.21 | 0.18 | 0.23 | 0.13 |
| CoV (%) | 14.8 | 14.8 | 14.8 | 14.8 | 15.2 | 15.2 | 14.8 | |
| 4d = 64 | 188a | 1.05 | 1.15 | 1.56 | 1.15 | 0.94 | 1.40 | 0.92 |
| | 188b | 1.11 | 1.21 | 1.65 | 1.21 | 0.99 | 1.48 | 0.97 |
| | 188c | 0.96 | 1.05 | 1.43 | 1.05 | 0.86 | 1.28 | 0.84 |
| | 188d | 1.10 | 1.20 | 1.64 | 1.20 | 0.98 | 1.47 | 0.97 |
| | 188e | 1.11 | 1.21 | 1.65 | 1.21 | 0.99 | 1.48 | 0.97 |
| | 187a | 1.14 | 1.25 | 1.70 | 1.25 | 1.02 | 1.52 | 1.00 |
| | 187b | 1.31 | 1.43 | 1.95 | 1.43 | 1.16 | 1.74 | 1.15 |
| | 187c | 1.11 | 1.22 | 1.66 | 1.22 | 0.99 | 1.48 | 0.98 |
| | mean | 1.11 | 1.21 | 1.66 | 1.22 | 0.99 | 1.48 | 0.97 |
| | SD | 0.10 | 0.11 | 0.15 | 0.11 | 0.09 | 0.13 | 0.09 |
| | CoV (%) | 8.9 | 8.9 | 8.9 | 8.9 | 8.7 | 8.7 | 8.9 |

Regarding the influence of loaded edge distance on the theoretical/experimental ratios, there seems to be a tendency for the mean ratio to increase as the distance increases from 2 to 3d for all models. However, in the case of the 4d distance, the ratio decreases to a greater

or lesser extent for most models. Even so, the magnitudes of the differences are not uniform. Uniformity of the trends of the theoretical/experimental ratio in relation to the loaded edge distance was also not found by Hindman et al. [52] using the models

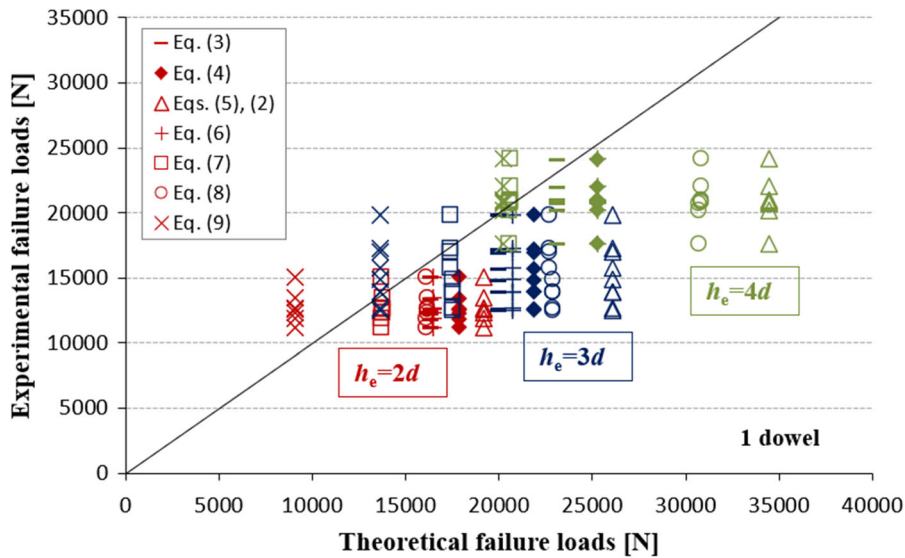


Fig. 6 Experimental versus theoretical failure loads predicted by the analytical models for single dowel connections

described in Eqs. (5) and (7) for beams with the same span/depth ratio as those studied in the present work.

Similarly, the ratios of the theoretically predicted failure loads to the experimental values of the specimens with double-dowel connections are presented in Table 6, together with the main values of each set of results.

A visual comparison of these failure loading ratios for the double-dowel connections is shown in Fig. 7,

where each symbol represents the ratio obtained using a different analytical model.

For this arrangement, the Eq. (7) based on quasi-nonlinear fracture mechanics and including tensile strength perpendicular to the grain, again stands out, being in this case the one that provides the most conservative predictions. In any case, it is worth noting that for the two-dowel configuration, there is a higher number of specimens giving ratios below 1 compared to the single dowel arrangements, although

Table 6 Theoretical vs. experimental failure load ratios of double-dowel connection tests

| h_e (mm) | name | Equation (3) | Equation (4) | Equation (2), Equation (5) | Equation (6) | Equation (7) | Equation (8) | Equation (9) |
|---------------|------------|--------------|--------------|-------------------------------|--------------|--------------|--------------|--------------|
| 4d = 64 | 183a | 1.11 | 1.21 | 1.66 | 1.59 | 0.98 | 1.47 | 1.39 |
| | 183b | 0.81 | 0.89 | 1.21 | 1.17 | 0.72 | 1.08 | 1.02 |
| | 183c | 0.95 | 1.04 | 1.42 | 1.37 | 0.85 | 1.27 | 1.20 |
| | 183d | 0.85 | 0.93 | 1.26 | 1.22 | 0.75 | 1.12 | 1.06 |
| | 183e | 0.75 | 0.83 | 1.13 | 1.08 | 0.67 | 1.00 | 0.94 |
| | 184a | 0.83 | 0.91 | 1.25 | 1.20 | 0.74 | 1.11 | 1.05 |
| | 187f | 0.92 | 1.01 | 1.37 | 1.32 | 0.82 | 1.22 | 1.15 |
| | 187g | 1.22 | 1.34 | 1.82 | 1.75 | 1.09 | 1.62 | 1.53 |
| | mean | 0.93 | 1.02 | 1.39 | 1.34 | 0.83 | 1.24 | 1.17 |
| | SD | 0.16 | 0.17 | 0.24 | 0.23 | 0.14 | 0.21 | 0.20 |
| | CoV (%) | 17.2 | 17.2 | 17.2 | 17.2 | 17.2 | 17.2 | 17.2 |



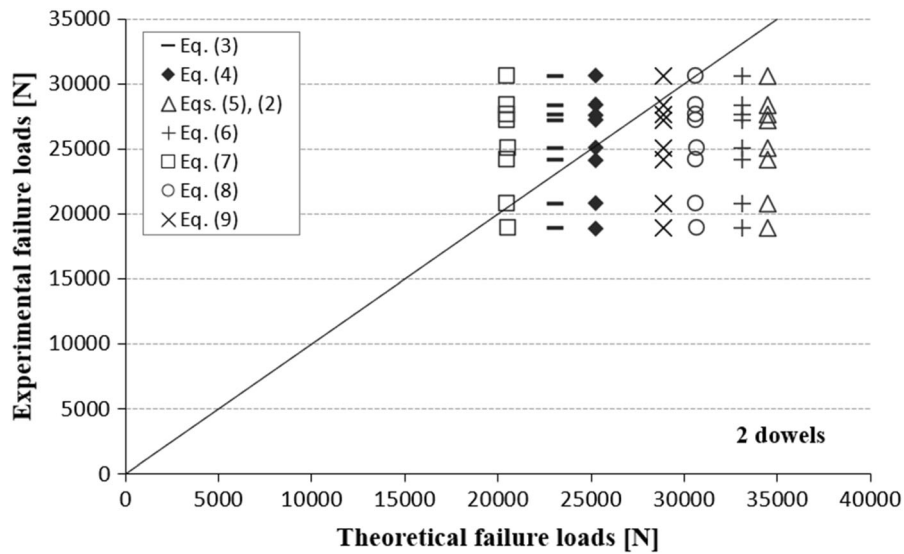


Fig. 7 Experimental versus theoretical failure loads predicted by the analytical models for double dowel connections

most analytical formulations were developed considering a single connector (and mostly softwoods).

Although all the models studied give load capacity predictions closer to the experimental values for beams with two dowels than for single dowels, Eqs. (2) and (5), the latter basis of the Eurocode 5 formula, are again the least appropriate for eucalyptus.

The models described by Eqs. (6) and (9) are the only ones in the studied that include some parameter related to the multiple dowel connection. In particular, Eq. (6) includes a correction factor for the splitting capacity to account for the influence of the connection width ($f_w = 1.31$ for the double connection studied), but also gives a poor prediction of the experimental values (ratio = 1.34, see Table 6). However, if this correction factor had not been considered, the average value of the experimental versus theoretical failure load ratio would result in 1.02, similar to the ratios obtained using Eq. (4), and therefore significantly better predictions than considering the correction factor.

In turn, Eq. (9) formulated by Franke and Quenneville, considering the mixed mode of fracture, again gives good estimates of the experimental values, as in the case of single bolt connections, although this formula was calibrated using spruce laminated beams [39] and extended to Radiata pine LVL [54].

The results suggest that more comprehensive analytical models, where more material parameters

are considered, such as Mode I and II fracture energies and tensile strength perpendicular to the grain, lead to more reliable predictions. In any case, further studies with different connection geometries and species and products should be performed to come up with an expression that can be optimally applicable to hardwoods.

4.3 Applicability of the Eurocode 5 expression

As mentioned above, a manifestation of Eq. (5) proposed by van der Put and Leijten [33] appears in Eurocode 5 [30] as a specific splitting capacity check for connections in softwoods loaded perpendicular to the grain (however, application to hardwoods and other wood-based products is not specified). It considers the verification of the shear force acting on the beam by the following expression,

$$F_{v,Ed} \leq F_{90,Rd} \tag{10}$$

being $F_{v,Ed} = \max(F_{v,Ed,1}, F_{v,Ed,2})$, where $F_{v,Ed,1}$ and $F_{v,Ed,2}$ are the design shear forces acting on both sides of the joint.

For softwoods connected by fasteners other than punched metal plates type, the characteristic value of the splitting load is described in the code as,

$$F_{90,Rk} = bC_1 \sqrt{\frac{h_e}{1 - \frac{h_e}{h}}} \tag{11}$$

where b and h are the width and depth of the beam, respectively, h_e is the distance from the loaded edge to the dowel location, and $C_1 = 14 \text{ N/mm}^{1.5}$. From its origins, this 14 value derives from what is known as the *apparent fracture parameter*, $(GG_c)^{0.5}$, which represents the square root of the shear modulus, G , times the critical energy release rate, G_c , in the form $C_1 = (GG_c/0.6)^{0.5}$.

The apparent fracture parameter was used by Van der Put and Leijten as a fitting parameter by taking test data from a limited number of sources with different connection types. The mean lower bound of the apparent fracture parameter of $12 \text{ N/mm}^{1.5}$ was selected, leading to a factor $C_1 = 15.5 \text{ N/mm}^{1.5}$. To obtain a characteristic value, the factor C_1 was further reduced to $15.5 \cdot 2/3 \approx 10 \text{ N/mm}^{1.5}$, and this was the value suggested for use in the code design criterion. Even so, the value finally adopted by Eurocode 5 was $C_1 = 14 \text{ N/mm}^{1.5}$, which corresponds to an apparent fracture parameter of $(GG_c)^{0.5} = 10.84 \text{ N/mm}^{1.5}$ ($= 14 \cdot 0.6^{0.5}$).

This apparent fracture energy parameter assumed in the expression of the European code has been discussed since its origins. Some studies suggest obtaining individual C_1 factors for each species [54] as G_I fracture energy values are not specified in Eurocode 5 or related product standards. Therefore, a comprehensive experimental determination of this parameter would be desirable for each species or wood product.

Proceeding in a similar way to that mentioned above, the values of factor C_1 of the Eurocode 5 formula that would correctly predict the experimental failure loads obtained for eucalyptus are shown in Table 7. As can be seen, the lowest characteristic value of factor C_1 (calculated as $2/3C_1$) results in $19.45 \text{ N/mm}^{1.5}$, which is 1.39 times the value established by Eurocode 5 for softwoods ($C_1 = 14 \text{ N/mm}^{1.5}$).

However, when considering the mean values of G and G_c obtained from the experimental tests on *Eucalyptus globulus* ($G_{LR} = 1926 \text{ MPa}$ and $G_{Ic} = 0.77 \text{ N/mm}$, respectively), the apparent fracture parameter $(GG_c)^{0.5}$ results in $38.51 \text{ N/mm}^{1.5}$. It leads to a $C_1 = 49.71 \text{ N/mm}^{1.5}$, which can be reduced by $2/3$ and gives the characteristic value of $33.14 \text{ N/mm}^{1.5}$, 2.37 times the value established by Eurocode 5 and higher than the value obtained from the process shown in Table 7. This high C_1 value of eucalyptus respond to the high performance of hardwoods compared to softwoods due to their anatomical differences.

The splitting capacity of the eucalyptus specimens was also predicted by directly applying the Eurocode 5 formula developed for softwoods (Eq. (11)), where $C_1 = 14 \text{ N/mm}^{1.5}$. The results are presented in Table 8. In this case, the design capacity does not explicitly depend on any material parameter. The only input parameters are the beam depth and width and the loaded edge distance from the dowel. The results were adjusted to the design values to account for the type of material, the duration of loading, and the effects of the moisture content ($k_{mod} = 0.9$ and $\gamma_M = 1.3$). Table 8 also includes the averages and CoV values of the design factor of safety (DFS) for each configuration, defined as the ratio of the test capacity strength to the Eurocode 5 design splitting capacity.

The DFS values generally ranged between 2.5 and 4.6, with no clear trend with respect to the loaded edge distance. Therefore, the prediction formula included in Eurocode 5 for softwoods is prone to underestimate the splitting capacity of the eucalyptus specimens, leading to very conservative predictions.

Table 7 Factor C_1 of Eq. (11) that would predict the experimental failure loads of eucalyptus

| | h_e (mm) | $(GG_c)^{0.5}$ ($\text{N/mm}^{1.5}$) mean | C_1 ($\text{N/mm}^{1.5}$) mean | C_1 ($\text{N/mm}^{1.5}$) characteristic |
|----------|------------|---|------------------------------------|--|
| 1 dowel | $2d = 32$ | 25.59 | 33.04 | 22.03 |
| | $3d = 48$ | 22.60 | 29.18 | 19.45 |
| | $4d = 64$ | 23.40 | 30.21 | 20.14 |
| 2 dowels | $4d = 64$ | 28.35 | 36.60 | 24.40 |



Table 8 Characteristic and design values of the eucalyptus splitting capacity applying the Eurocode 5 expression and design factors of safety (DFS)

| | h_e (mm) | $F_{90,R,k}$ (kN) | $F_{90,R,d}$ (kN) | DFS (mean) | CoV (%) |
|----------|------------|-------------------|-------------------|------------|---------|
| 1 dowel | $2d = 32$ | 2.70 | 1.87 | 3.4 | 9.8 |
| | $3d = 48$ | 3.67 | 2.54 | 3.0 | 15.7 |
| | $4d = 64$ | 4.85 | 3.36 | 3.1 | 8.6 |
| 2 dowels | $4d = 64$ | 4.85 | 3.36 | 3.8 | 15.6 |

5 Conclusions

The results of the splitting capacity of *Eucalyptus globulus* L. beams loaded perpendicular to the grain by single and double steel dowel connections with different loaded edge distances are provided. These are essential preliminary data to gain knowledge on the splitting behaviour in hardwoods as there is no specific equation for its prediction included in Eurocode 5, only for softwoods.

From the experimental study for the geometry of the tested beam, the load carrying capacity considering a single dowel increases with increasing distance to the loaded edge. Distances of $4d$ result in ductile failures and smaller distances in brittle failures. However, in the case of two dowels at $4d$, the load carrying capacity is similar to that of one dowel and the failure is clearly brittle. This is of particular relevance, as the Eurocode 5 formula does not take into account the number of dowels.

Of the eight analytical models based on fracture mechanics studied (including the model basis of the Eurocode 5 formula) and considering the actual eucalyptus properties required as input of these models, in general, all of them overestimate the splitting failure load of single-dowel eucalyptus beams, except the only model that considers Mode II fracture energy in addition to Mode I fracture energy in its expression. For the double dowel layout, an analytical model based on quasi-nonlinear fracture mechanics, which also includes the tension perpendicular to grain of the member, provides the most conservative predictions and also good agreement for the single dowel beams. In all arrangements, the analytical model basis of the Eurocode 5 expression gives the worst agreement with the experimental eucalyptus results.

The splitting capacity formula adopted by Eurocode 5 for softwoods, which does not take into account any material parameter, only the depth and width of the beam and the distance from the dowel to the loaded edge, proves to be very conservative in predicting the ultimate failure load of *Eucalyptus globulus* with the connection geometries analysed in this study.

Further experimental research on the splitting behaviour of this and other hardwood species would be desirable in order to derive an optimal general formula valid for all of them, taking into account the different material properties, as well as the geometry and type of connection.

Acknowledgements This work was supported by an STSM grant from COST Action FP1402 *Basis of Structural Timber Design—from research to standards*. The work is part of the R&D&I Project BIA2015-64491-P funded by MCIN/AEI/“<http://sci-hub.tw/10.13039/501100011033>” target=“_blank”>10.13039/501100011033 and by ERDF A way of making Europe. Fundação para a Ciência e a Tecnologia (FCT-MCTES) is acknowledged for the financial support of the Research and Development Unit for Mechanical and Industrial Engineering (UNIDEMI) by the project UIDB/00667/2020.

Funding Open Access funding provided thanks to the CRUE-CSIC agreement with Springer Nature.

Declarations

Conflict of interest The authors declare that they have no conflict of interest.

Open Access This article is licensed under a Creative Commons Attribution 4.0 International License, which permits use, sharing, adaptation, distribution and reproduction in any medium or format, as long as you give appropriate credit to the original author(s) and the source, provide a link to the Creative Commons licence, and indicate if changes were made. The images or other third party material in this article are included in the article’s Creative Commons licence, unless indicated otherwise in a credit line to the material. If material is not included in the article’s Creative Commons licence and your intended use is not permitted by statutory regulation or exceeds



the permitted use, you will need to obtain permission directly from the copyright holder. To view a copy of this licence, visit <http://creativecommons.org/licenses/by/4.0/>.

References

- Aicher S, Christian Z, Dill-Langer G (2014) Hardwood glulams—emerging timber products of superior mechanical properties. In: Proceedings of the World Conference on Timber Engineering (WCTE2014), Quebec City, Canada
- Z-9 (2019) 1–679: allgemeine bauaufsichtliche Zulassung für BS-Holz aus Buche und BS-Holz Buche-Hybridträger und zugehörige Bauarten, Deutsches Institut für Bautechnik (DIBt), Antragsteller: Studiengemeinschaft Holzleimbau e.V., Wuppertal, Germany
- ETA-13/0646 (2018) SIEROLAM—Glued laminated timber of chestnut. European Technical Approval, Österreichisches Institut für Bautechnik (OIB); Holder: SIEROLAM S.A., Siero, Spain
- ETA-13/0642 (2018) VIGAM – Glued laminated timber of oak, European technical approval, Österreichisches Institut für Bautechnik (OIB); Holder: Elaborados y Fabricados Gamiz S.A., Sta. Cruz de Campezo, Spain
- McGavin RL, Bailleres H, Hamilton M, Blackburn D, Vega M, Ozarska B (2015) Variation in rotary veneer recovery from Australian plantation *Eucalyptus globulus* and *Eucalyptus nitens*. *BioRes* 10(1):313–329
- Franke S, Marto J (2014) Investigation of Eucalyptus globulus wood for the use as an engineered material. In: World Conference on Timber Engineering (WCTE2014), Quebec City, Canada.
- Navarrete E, Valenzuela C, Nutto L (2016) Modeling the effect of pruning and thinning on growth strain of *Eucalyptus globulus* Labill. *Ciência Florest* 26(3):901–912.
- Wiseman D, Pinkard E, Wardlaw T, Mohammed C, Hall M, Beadle C (2009) Growth responses of Eucalyptus globulus and E. nitens to pruning and fertiliser treatments in a plantation managed for solid-wood products. *South Forests A J Forest Sci* 71(1):21–29.
- Crespo J, Aira JR, Vázquez C, Guaita M (2017) Comparative analysis of the elastic constants measured via conventional, ultrasound, and 3-D digital image correlation methods in *Eucalyptus globulus*. *Bioresources* 12:3728–3743
- Crespo J, Majano-Majano A, Lara-Bocanegra AJ, Guaita M (2020) Mechanical properties of small clear specimens of *Eucalyptus globulus* Labill. *Materials* 13:906.
- Lara-Bocanegra AJ, Majano-Majano A, Arriaga F, Guaita M (2020) Eucalyptus globulus finger jointed solid timber and glued laminated timber with superior mechanical properties: characterisation and application in strained gridshells. *Constr Build Mater* 265:120355.
- Fernández-Golfín JI, Díez R, Hermoso E, Baso C, Casas JM, González O (2007) Caracterización de la madera de Eucalyptus globulus para uso estructural. *Bol Inf CIDEU* 4:91–100 ((in Spanish))
- Lara-Bocanegra AJ, Majano-Majano A, Crespo J, Guaita M (2017) Finger-jointed *Eucalyptus globulus* with 1C-PUR adhesive for high performance engineered laminated products. *Constr Build Mater* 135:529–537.
- López-Suevos F, Richter K (2009) Hydroxymethylated resorcinol (HMR) and novolak-based HMR (n-HMR) primers to enhance bond durability of Eucalyptus globulus glulams. *J Adhes Sci Technol* 23(15):1925–1937.
- Martins C, Dias AMPG, Cruz H (2020) Blue gum: assessment of its potential for glued laminated timber beams. *Eur J Wood Prod* 78:905–913.
- Ettelaei A, Taoum A, Nolan G (2021) Rolling shear properties of cross-laminated timber made of fibre-managed plantation eucalyptus under short-span bending. *Wood Mater Sci Eng.*
- Pangh H, Hosseinabadi HZ, Kotlarewski N, Moradpour P, Lee M, Nolan G (2019) Flexural performance of cross-laminated timber constructed from fibremanaged plantation eucalyptus. *Constr Build Mater* 208:535–542.
- Gilbert BP (2018) Compressive Strength Prediction of Veneer-Based Structural Products. *J Mater Civ Eng* 30(9):04018225
- Gilbert BP, Husson JM, Bailleres H, McGavin RL, Fischer MF (2018) Perpendicular to grain and shear mechanical properties of veneer-based elements glued from single veneer sheets recovered from three species of juvenile subtropical hardwood plantation logs. *Eur J Wood Prod* 76:1637–1652.
- Gilbert BP, Bailleres H, Fischer MF, Zhang H, McGavin RL (2017) Mechanical properties of rotary veneers recovered from early to midrotation subtropical-hardwood plantation logs for veneer-based composite applications. *J Mater Civ Eng* 29(10):04017194.
- Derikvand M, Jiao H, Kotlarewski N, Lee M, Chan A, Nolan G (2019) Bending performance of nail-laminated timber constructed of fast-grown plantation eucalypt. *Eur J Wood Prod* 77:421–437.
- Legg P, Frakes I, Gavran M (2021) Australian plantation statistics and log availability report 2021. ABARES research report, Canberra.
- Tomé M, Almeida MH, Barreiro S, Branco MR, Ernesto Deus E, Glória Pinto G, Silva JS, Soares P, Rodríguez-Soalleiro R (2021) Opportunities and challenges of Eucalyptus plantations in Europe: the Iberian Peninsula experience. *Eur J Forest Res* 140:489–510.
- EN 1912 (2012) Structural timber. Strength classes. Assignment of visual grades and species. European Committee for Standardization
- UNE 56546 (2013) Visual grading for structural sawn timber. Hardwood timber. Asociación Española de Normalización y Certificación. (In Spanish)
- Lara-Bocanegra AJ, Majano-Majano A, Arriaga F, Guaita M (2018) Long-term bending stress relaxation in timber laths for the structural design of lattice shells. *Constr Build Mater* 193:565–575.
- Johansen KW (1949) Theory of Timber Connections. *Publ Int Assoc Bridge Struct Eng* 9:249–262
- DIN 1052 (2008) Entwurf, Berechnung und Bemessung von Holzbauwerken - Allgemeine Bemessungsregeln und Bemessungsregeln für den Hochbau. Deutsches Institut für Normung, Berlin, Germany
- Ehlbeck J, Görlacher R, Werner H (1989) Determination of perpendicular to grain stresses in joints with dowel-type



- fasteners - A draft proposal for design rules. In: Proc of the CIB-W18 meeting 22, Berlin, Germany, Paper No. CIB-W18/22-7-2.
30. EN 1995-1-1 (2016) Eurocode 5: Design of timber structures. part 1-1: General. Common rules and rules for buildings. European Committee for Standardization
 31. CSA O86:19(2019) Engineering design in wood. Canadian Standards Association. Toronto, Canada
 32. Van der Put TACM (1990) Tension perpendicular to grain at notches and joints. In: Proc. of the CIB-W18 Meeting 23, Lisbon, Portugal, Paper No. CIB-W18/23-10-1
 33. Van der Put TACM, Leijten AJM (2000) Evaluation of perpendicular to grain failure of beams caused by concentrated loads of joints. In: Proc. of the CIB-W18 Meeting 33, Delft, The Netherlands, Paper No. CIB-W18/33-7-7
 34. Jensen JL (2005) Splitting strength of beams loaded perpendicular to grain by dowel joints. *J Wood Sci* 51(5):480-485.
 35. Jensen JL, Quenneville P, Girhammar UA, Källsner B (2015) Brittle failures in timber beams loaded perpendicular to grain by connections. *J Mater Civ Eng* 27(11):04015026.
 36. Larsen HJ, Gustafsson PJ (2001) Dowel joints loaded perpendicular to grain. Proc. of the CIB-W18 Meeting 34, Venice, Italy, Paper No. CIB-W18/34-7-3.
 37. Ballerini M (2004) A new prediction formula for the splitting strength of beams loaded by dowel-type connections. In: Proceeding of the CIB-W18 Meeting 37, Edingburgh, Scotland, Paper No. CIB-W18/37-7-5.
 38. Jensen JL (2005) Quasi-non-linear fracture mechanics analysis of the splitting failure of single dowel joints loaded perpendicular to grain. *J Wood Sci* 51:559-565.
 39. Franke B, Quenneville P (2011) Design approach for the splitting failure of dowel-type connections loaded perpendicular to grain. In: Proceeding of the CIB-W18 Meeting 44, Alghero, Italy. Paper No. CIB-W18/44-7-5.
 40. Jensen JL, Quenneville P, Girhammar UA, Källsner B (2012) Splitting of timber beams loaded perpendicular to grain by connections - combined effect of edge and end distance. *Constr Build Mater* 35:289-293.
 41. Schoenmakers JCM (2010) Fracture and failure mechanisms in timber loaded perpendicular to grain by mechanical connections. In: PhD Thesis, University of Technology, Eindhoven, The Netherlands.
 42. Jockwer R, Dietsch P (2018) Review of design approaches and test results on brittle failure modes of connections loaded at an angle to the grain. *Eng Struct* 171:362-372.
 43. Crespo J, Majano-Majano A, Xavier J, Guaita M (2018) Determination of the resistance-curve in *Eucalyptus globulus* through double cantilever beam tests. *Mater Struct* 51:77.
 44. Majano-Majano A, Lara-Bocanegra AJ, Xavier J, Morais J (2019) Measuring the cohesive law in Mode I loading of *Eucalyptus globulus*. *Materials* 12:23.
 45. Majano-Majano A, Lara-Bocanegra AJ, Xavier J, Morais J (2020) Experimental evaluation of Mode II fracture properties of *Eucalyptus globulus* L. *Materials* 13:745.
 46. EN 408 (2011) Timber structures - structural timber and glued laminated timber - determination of some physical and mechanical properties. European Committee for Standardization.
 47. Gustafsson P (2003) Fracture perpendicular to grain - Structural applications. In: Landersson S, Larsen HJ (eds) Timber engineering. Wiley, Chichester
 48. Ballerini M, Rizzi M (2007) Numerical analyses for the prediction of the splitting strength of beams loaded perpendicular-to-grain by dowel-type connections. *Mater Struct* 40:139-149.
 49. Quenneville JHP, Mohammad M (2001) Design method for bolted connections loaded perpendicular-to-grain. *Can J Civ Eng* 28:949-959.
 50. Reshke R (1999) Bolted timber connections loaded perpendicular-to-grain: influence of joint configuration parameters on strength. In: M.Sc. Thesis, Department of Civil Engineering, Royal Military College of Canada, Kingston, Ontario.
 51. Kasim M, Quenneville P (2002) Effect of row spacing on the capacity of bolted timber connections loaded perpendicular-to-grain. In Proceeding of the CIB-W18 meeting, Kyoto, Japan, Paper No. CIB-W18/35-7-6.
 52. Hindman DP, Finkenbinder DE, Loferski JR, Line P (2010) Strength of sawn lumber and wood composite connections loaded perpendicular to grain. II: fracture mechanics equations. *J Mater Civ Eng* 22(12):1226-1234.
 53. Patel MC, Hindman DP (2012) Comparison of single- and two-bolted LVL perpendicular-to-grain connections. II: Fracture models. *J Mater Civ Eng* 24(4):347-355.
 54. Franke B, Quenneville P (2012) Prediction of the load capacity of dowel-type connections loaded perpendicular to grain for solid wood and wood products. In: Proceedings of the World Conference of Timber Engineering (WCTE), Auckland, New Zealand

Publisher's Note Springer Nature remains neutral with regard to jurisdictional claims in published maps and institutional affiliations.

